BRAIN TUMOR VASCULAR NETWORK SEGMENTATION FROM MICRO-TOMOGRAPHY

Xavier Descombes[1], *Franck Plouraboué*[2], *Abdelhakim El Boustani*[2,3], *Caroline Fonta*[4]
Géraldine LeDuc[5], *Raphael Serduc*[5], *Timm Weitkamp*[5] *

[1] INRIA/I3S, 2004 route des Lucioles, BP93, 06902 Sophia Antipolis Cedex, France
[2] IMFT UMR 5502 CNRS/INPT/UPS, av. du Pr. Camille Soula, 31400 Toulouse, France
[3] Ecole Nationale des Sciences Appliques de Tanger (ENSA), BP 1818, Tanger, Morocco
[4] Univ. Toulouse, UPS, Centre de Rech. Cerveau et Cognition / CNRS, CerCo, 31410 Toulouse, France
[5] ESRF, 6 rue Jules Horowitz, BP220, 38043 Grenoble Cedex 9, France

ABSTRACT

Micro-tomography produces high resolution images of biological structures such as vascular networks. In this paper, we present a new approach for segmenting vascular network into pathological and normal regions from considering their micro-vessel 3D structure only. We define and use a conditional random field for segmenting the output of a watershed algorithm. The tumoral and normal classes are thus characterized by their respective distribution of watershed region size interpreted as local vascular territories.

***Index Terms*—** Segmentation, conditional random field, micro-tomography, brain tumor

1. INTRODUCTION

High resolution micro-tomography provides an efficient imaging technique for the systematic 3D analysis of supracellular structures such as micro-vascular networks [1, 2]. Since the diameters of most capillary vessels are distributed between 5 and 9 microns, micrometric spatial resolution is necessary for such a method to capture the entire vascular network.

Specific 3-D images of vessel networks can be obtained from the injection of an X-ray contrast agent in various tissues [1]. It brings to the fore specific features of normal or pathological vessels, as for example in the brain [3]. To be more precise, tumorous vessels are large, irregular and tortuous, compared to normal ones in most tumors and organs. As opposed to classical microscopic studies, the scale of analysis in CT-volumes is different from single cell, thus providing important organizational level of information. At the millimeter scale, the number of vessels is very important, so that it is not reasonable to perform manually any vessel segmentation. It is thus necessary to develop automatic segmentation methods for a systematic, quantitative, reliable and differentiated investigation of normal and pathological networks. Such segmentation allows ultimately a detailed comparison between normal and pathological vessels with respect to their shape and spatial distribution as well as the determination of the angiogenic regions of a given tumor. A reliable automated segmentation would be of high interest because there is indeed a growing evidence in the recent literature [4] that the maturation and maybe the normalization of tumoral vascular networks may be related to the observed resistance of the brain tumors to various treatments [5].

In this paper, we propose a segmentation method adapted to normal/tumorous vessel networks. We consider binary volumes composed of a background and a 3D network representing the vessels. The binarization is performed using an hysteresis thresholding (see [3]) and is robust since the tomographic data are very contrasted. Our objective is to find a criterion to segment this network in two classes. From a careful inspection of the obtained image of vessels, it is clear that in the tumoral region the vessels are larger, very irregular, with complex shape quite different from the smooth elongated cylinders observed in normal regions. This observation suggests that vessel shape could be used to distinguish normal and pathological regions. Nevertheless, the automatic skeletonization of the vessels is very time consuming. Furthermore the quality of this skeletonization largely depends on the vessel smoothness (the thinning step of most skeletonization procedures is not robust when irregular shapes are present). Hence, it is neither easy nor computationally efficient to use vessel shape as a segmentation criteria. Fortunately another important property of tumorous vessels can be observed : the vessels in the tumor are further apart from each other [3]. The local vessel territories can thus be used for segmenting the vessel network.

We therefore quantify this sparsity for segmenting the network as being the main differentiating structural property. We first partition the volume into regions associated to local vascular territories using a watershed algorithm. Then we segment the full partitioned volume based on the size of each

*This research was supported by the ANR project "Micro-Réseaux".

partitioned 3D region, which exhibits different distribution in normal and pathological tissues. The different steps of the methods are detailed in section 2.

To segment the partitioned volume, we consider the graph where each vertex represents a region and edges are defined between adjacent regions. We show that the watershed region distribution follows a power-law tailed Pareto law leading to noisy segmentation when considering a maximum likelihood estimator. We therefore regularize the solution by introducing a conditional random field, detailed in section 3. Finally, the segmentation results are described in section 4.

2. METHOD

We start with binarized volumes (micro-vascular networks images are highly contrasted and easy to binarize). A dataset consists of several sub-volumes, which may have different sizes. For segmenting the entire volume, we consider the following steps:

Closing- On each sub-volume, a closing with a ball as a structuring element is applied. The radius of the ball is 4 voxels. This pre-processing step aims to repair vessels which may have been split into different connected components during the binarization process. The closing step cleans the data for the next step.

Down-sampling- We then merge the different sub-volumes. However, in order to restrain the need for memory allocation, we have to down-sample the different sub-volumes. We associate a single voxel to each $3 \times 3 \times 3$ cube of the initial data, before merging the sub-volumes. To avoid disconnecting vessels, we assign value 1 (vessel) to each voxel in the down-sampled volume for which at least one of the voxels on the corresponding cube at the initial resolution belongs to vessels.

Registration and merging- The merging step is performed by registering the sub-volumes. We only have to estimate a translation vector between two overlapping sub-volumes. This vector is computed by maximizing the number of common voxels marked as vessels. An example of a full volume is shown on figure 1

Distance map- A distance map is computed from calculating the Euclidean distance in 3D from each nearest vessel.

Watershed- We compute the watershed of the inverse of the distance map, shown on figure 2. The result is displayed on figure 3. Since it is expected that the tumor is surrounded by vessels, the vessels are localized on the boundaries of watershed regions.

Labeling- We label the watershed regions into tumor and non tumor areas. We develop an original model based on a Conditional Random Field on a graph which is detailed in section 3. The segmentation obtained is shown in figure 4.

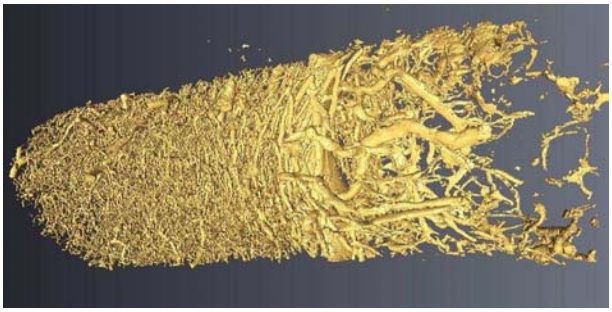

Fig. 1. volume rendering of the full volume of data after the merging step

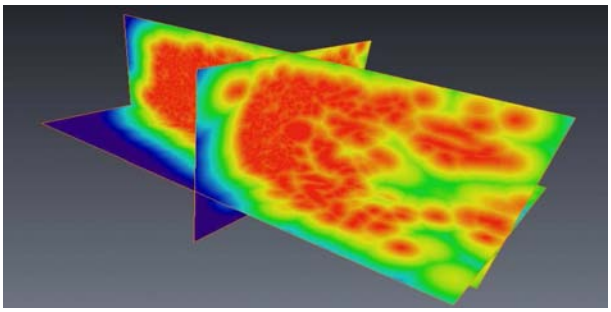

Fig. 2. Distance map to any vessel

3. A CONDITIONAL RANDOM FIELD ON THE WATERSHED GRAPH

In this section, we detail the graph labeling algorithm based on a Conditional Random Field (CRF) that we propose for segmenting the tumor.

We consider a graph $\mathcal{G}$, derived from the partitioned volume issued from the watershed algorithm. Each region of the watershed result is considered as a vertex i if it is not connected to the volume boundary. The set of vertices is denoted by $\mathcal{I}$. The edges are defined by the following neighborhood relation: $i \sim j$ if and only if i and j correspond to two connected regions.

We label the graph $\mathcal{G}$ by $g_i = 1$ for tumor regions and $g_i = 0$ for non-pathological regions. The resulting information is the region size s_i and some prior knowledge on the connectivity of the tumor. To embed these two informations into a single model we consider a binary Conditional Random Field on the graph $\mathcal{G}$. Conditional random fields can be seen as an extension of the standard Markov Random Field approach based on the Bayes formalism [6, 7]. The posterior is directly modeled instead of defining it through the product of a prior and a likelihood. In our context, this allows normalizing the weight of the data term and the interaction potentials independently of the local topology of the graph.

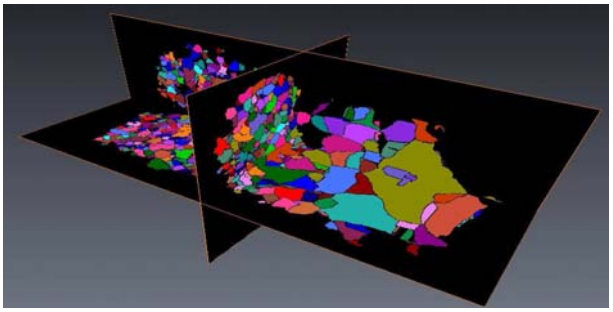

Fig. 3. Watershed on the distance map opposite

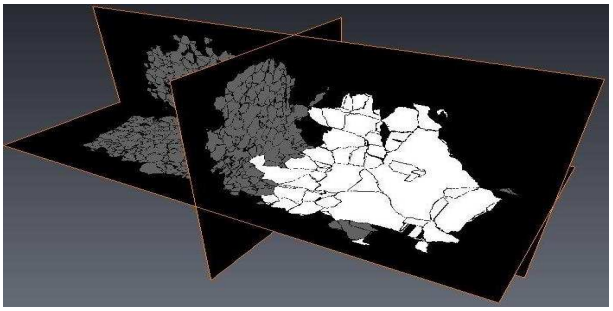

Fig. 4. Segmentation: tumor (white) and normal tissue (grey)

3.1. Likelihood definition

To define the likelihood we consider two sub-volumes, V_t and V_s, corresponding to tumor and normal tissues respectively. The empirical volume distribution of both classes exhibits a heavy tail behavior. Consistently, the log-log histograms display a linear behavior leading to Pareto parameters estimation. We successfully tested the Pareto distribution hypothesis using the Kolmogorov-Smirnov test, ($p = 0.06$ for the empirical tumor volume distribution and $p = 4.10^{-8}$ for normal tissue).

Therefore, we consider the following likelihood :

$$\begin{cases} p(s_i|g_i = 1) = \beta_t s_i^{-\alpha_t} & \text{if } s_i < \min_t \\ p(s_i|g_i = 1) = 0 & \text{otherwise} \end{cases} \quad (1)$$

and

$$\begin{cases} p(s_i|g_i = 0) = \beta_s s_i^{-\alpha_s} & \text{if } s_i < \min_s \\ p(s_i|g_i = 0) = 0 & \text{otherwise} \end{cases} \quad (2)$$

where α_t, β_t (resp. α_s, β_s) are the parameters of the likelihood of tumor (resp. normal tissue). The minima are obtained through normalization of the distributions to 1, i.e. $\min = ((\alpha - 1)/\beta))^{\frac{1}{-\alpha+1}}$. To estimate these parameters, we first discretize the volume space on the logarithm scale and then apply a linear regression in the log-log domain. On the considered volumes, the regression gives $\alpha_s = 2.909$ and $\log(\beta_s) = 16.05$ for the normal tissue and $\alpha_t = 1.791$ and $\log(\beta_t) = 5.174$ for tumor. Let us consider the maximum classification shown in figure 5. The two classes are obviously mixed due to the overlapping between the tumor and normal class distributions. Moreover, the heavy tail of the normal class distribution is under the tumor class distribution, so that the tumor class tends to be overestimated by the maximum likelihood estimator. Therefore, a local filter is not sufficient to de-noise the maximum likelihood segmentation but a global model is necessary to regularize the result.

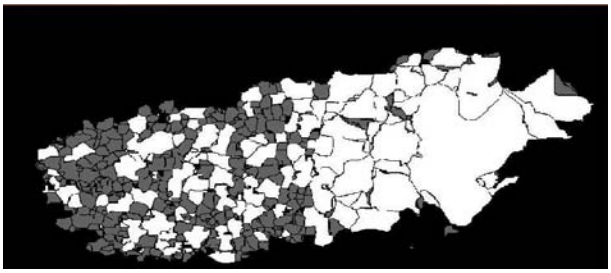

Fig. 5. Maximum likelihood using Pareto distributions

3.2. Posterior distribution

To regularize the solution, we consider a generalization of the Ising model [8]. Here we have to take into account two distinct properties. First, the number of neighbors of a given vertex is not constant. Besides, the size of neighbor region is also spatially variable. Therefore, we extend the Ising model by considering an attractivity property proportional to the contact surface between two regions as proposed in [9]. Therefore, small regions have a low impact on their neighbors. However, using this principle, the weight of the regularization term with respect to the data term depends on the size of the region. This may prevent regularization for small regions. Besides, the likelihood defined by Pareto distribution is equal to zero for small regions. To overcome this problem we consider a Conditional Random Field by directly addressing the posterior as follows

$$P(G = g|s) = \frac{1}{Z} \exp\left[-\beta \sum_{\{i,j\}:i\sim j} \mathrm{Surf(i,j)} \delta_{\mathrm{g_i \neq g_j}} - \sum_i \sum_{j:j\sim i} \mathrm{Surf(i,j)f(\log(p(s_i|g_i)))} \right], \quad (3)$$

where $\mathrm{Surf(i,j)}$ is the contact surface between regions i and j and:

$$f(\log(p(s_i|g_i))) = \begin{cases} \log(p(s_i|g_i)) & \text{if } p(s_i|g_i) \neq 0 \\ \mathrm{M} & \text{otherwise} \end{cases} \quad (4)$$

We maximize the posterior with a Metropolis dynamic embedded into a simulated annealing scheme [8].

4. RESULTS

We consider real intra-cortical images obtained using synchrotron tomography imaging at the European Synchrotron Radiation Facility (ESRF) [1, 10]. They consist of rat brain implanted with 9L gliosarcoma cells. The resolution is about one micron and a dataset represents about 8mm^3. The reconstructed image is first binarized using hysteresis thresholding and mathematical morphological open/closure procedures. The segmentation result obtained for $\beta = 5$, is shown on figure 6. The tumor segmentation in green corresponds to the experts expectation. It can provide statistical information about the vascular network characteristics. First, we can more precisely evaluate the Pareto distribution parameters. We obtain $\alpha_s = 3.089$ and $\log(\beta_s) = 18.79$ for the normal tissue and $\alpha_t = 1.524$ and $\log(\beta_t) = 3.420$ for tumor. This new estimation is stable when performing a new segmentation using these parameters. We also show the difference between the two vascular networks by computing the vessel diameter histograms (see figure 7, H_0 hypothesis rejected with p-value $2.2e-16$ using KS test) and the average vessel density (4.7% of vessel voxels for normal tissue versus 7.4% for tumor). Similar results have been obtained on six volumes representing a tumor at different stages. We are currently conducting a statistical study.

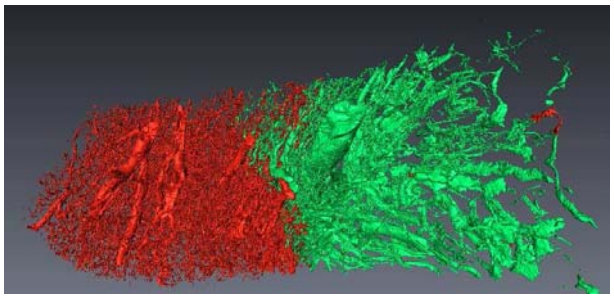

Fig. 6. Result: normal tissue (red) and tumor (green) ($\beta = 5$)

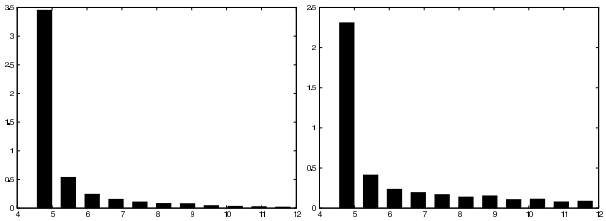

Fig. 7. Vessel diameter distribution, in micron, for normal tissue (left) and tumor (right)

5. CONCLUSION

In this paper, we have proposed a new approach for the segmentation of vascular networks, consisting of a CRF segmentation based on the watershed graph of the vessel tree. We have shown that this methods permits to segment tumourous and normal brain vascular networks. We found that both regions exhibit different statistical properties (vascular density and vessel diameter). In future work, we can extend this segmentation to a larger number of classes, as for example being able to evaluate tumor necrotic regions or hyper-vascular hot spots at the tumor border.

6. REFERENCES

[1] F. Plouraboué, P. Cloetens, C. Fonta, A. Steyer, F. Lauwers, and J. Marc-Vergnes, "High resolution x-ray imaging of vascular networks," *J. Microscopy*, vol. 215, no. 2, pp. 139–148, 2004.

[2] J. Reichold, M. Stampanoni, A.L. Keller, A. Buck, P. Jenny, and B. Weber, "Vascular graph model to simulate the cerebral blood flow in realistic vascular networks," *J. Cer. Blood Flow and Metab.*, vol. 29, pp. 1429–1443, 2009.

[3] L. Risser, F. Plouraboué, A. Steyer, P. Cloetens, G. Le Duc, and C. Fonta, "From homogeneous to fractal normal and tumorous micro-vascular networks in the brain," *J. Cer. Blood Flow and Metab.*, vol. 27, pp. 293–303, 2007.

[4] R.K. Jain, "Normalization of tumor vasculature : an emerging concept in angiogenic therapy," *Science*, vol. 307, pp. 58–62, 2005.

[5] R. Grépin and G. Pagès, "Molecular mechanisms of resistance to tumour anti-angiogenic strategies," *J. of Oncology*, 2010.

[6] J. Lafferty, A. McCallum, and F. Pereira, "Conditional random fields: probabilistic models for segmenting and labeling sequence data," in *Proc. 18th ICML*, 2001, pp. 282–289.

[7] S. Kumar and M. Hebert, "Discriminative random fields," *Int. J. Computer Vision*, vol. 68, no. 2, pp. 179–201, 2006.

[8] S. Geman and D. Geman, "Stochastic relaxation, Gibbs distributions, and the Bayesian restoration of images," *IEEE Trans. on PAMI*, vol. 6, pp. 721–741, 1984.

[9] T. Géraud, J-F. Mangin, I. Bloch, and H. Maître, "Segmenting internal structures in 3d mr images of the brain by markovian relaxation on a watershed based adjacency graph," in *Proc. 18th ICIP*, 1995, vol. 3, pp. 3548–3552.

[10] T. Weitkamp, P. Tafforeau, E. Boller, P. Cloetens, J.-P. Valade, P. Bernard, F. Peyrin, W. Ludwig, L. Helfen, and J. Baruchel, "Status and evolution of the esrf beamline id19," in *Proc. AIP Conf.*, 2010, vol. 1221, pp. 33–38.